

Photometric Invariant Region Detection

Theo Gevers, Arnold W.M. Smeulders and Harro Stokman
ISIS, University of Amsterdam, Kruislaan 403
1098 SJ Amsterdam, The Netherlands
[gevers | smeulders | stokman]@wins.uva.nl

Abstract

In this paper, we concentrate on determining homogeneously colored regions invariant to surface orientation change, illumination, shadows and highlights.

To this end, the influence of various well-known color models (e.g. I , RGB , XYZ , $I_1I_2I_3$, rgb , xyz , $U^*V^*W^*$, $L^*a^*b^*$ and ISH) are examined, in theory, for the dichromatic reflection model and, in practice, for two distinct region-based segmentation methods: the k-means clustering technique and the split&merge algorithm. Experiments are conducted on color images taken from colored objects in real-world scenes.

On the basis of the theoretical and experimental results it is concluded that $l_1l_2l_3$, H , S , $c_1c_2c_3$, rgb and xyz all detect regions invariant to a change in surface orientation, viewpoint of the camera, and illumination intensity. Furthermore, $l_1l_2l_3$ and H also detect regions independent of highlights. I , RGB , CMY , YIQ , XYZ , and $I_1I_2I_3$ provide segmentation results which are all sensitive to surface orientation and illumination intensity as well as color models incorporating brightness into their systems: I in HSI , L^* in $L^*a^*b^*$, and L in Luv .

1 Introduction

In the past, various color image segmentation methods have been proposed which do not account for the image formation process, [2], [8], for example. A major drawback of these color segmentation methods is that the values of the color features, on which the segmentation method relies, depend on the geometry of the object, the viewpoint of the camera or the illumination conditions. As a consequence, the obtained segmentation results are negatively affected by shadows, shading and highlights. In contrast, color segmentation methods that account for the process of image formation are studied recently. One of the first methods based on physics considerations is Klinker *et al.* [7]. They developed a clever color segmentation algorithm based on the dichromatic reflection model proposed by Shafer [9]. The method is based on evaluating "dog-leg" clusters in RGB -space. Then follows segmentation independent of the object's geometry, illumination and highlights. To achieve robust image segmentation, however, surface patches of objects in view must have a rather broad distribution of surface normals which may not be hold for objects in general. Bajscy *et al.* [1] developed a similar image segmentation method using the $H-S$ color space instead of the RGB -color space. Healey[5] proposes a method to segment images on the basis of normalized color. However, as normalized color is sensitive to highlights, a separate highlight removal technique should be applied on the image prior to

the actual segmentation. Various color features have been studied using a multi-resolution segmentation method [8]. However, no (reflection) model of the color imaging process is considered to explain the observed effects.

From the arguments mentioned so far, it follows that the choice of color models is of great importance for the purpose of proper image segmentation. It induces the equivalence classes to the actual segmentation algorithm. Therefore, in this paper, color models are studied for the purpose of color image segmentation on the basis of physics considerations. To this end, various well-known color features are analyzed in theory for the dichromatic reflection model and white illumination. Then, in practice, the behavior of the different color models are examined for two distinct region-based segmentation methods: a clustering and a region growing technique. The clustering technique is based on the k-means algorithm. The region growing technique is derived from the split&merge algorithm. In the evaluation, color images are taken from full-color objects in real-world scenes where objects were composed of a large variety of materials including plastic, textile, paper, wood, rubber, painted metal, ceramic and fruit.

The paper is organized as follows. In Section 2, the dichromatic reflection model under white illumination is given. The reflection model is used to study and analyze the RGB -subspace on which colors will be projected from an uniformly painted surface patch. In Section 3, the two region-based segmentation methods are discussed. Experiments carried out on the two segmentation methods will be given in Section 4. Finally, conclusions will be drawn.

2 Photometric Color Invariance

In this section, we briefly summarize and extend the theory that we have recently proposed on color invariant models, see [3] for example.

2.1 Color Models

Commonly used well-known color spaces include: (for display and printing processes) RGB , CMY (for television and video) YIQ , YUV , (standard set of primary colors) XYZ , (uncorrelated features) $I_1I_2I_3$, (normalized color) rgb , xyz , (perceptual uniform spaces) $U^*V^*W^*$, $L^*a^*b^*$, Luv and (for humans) HSI . Although, the number of existing color spaces is large, a number of these color models are correlated to intensity I : Y , L^* and W^* ; are linear combinations of RGB : CMY , XYZ and $I_1I_2I_3$; or normalized with respect to intensity rgb : IQ , xyz , UV , U^*V^* , a^*b^* , uv . Therefore, in this section, we concentrate on the following standard, *essentially different*, color features derived from RGB : intensity $I(R, G, B) = R + G + B$, RGB , normalized colors $r(R, G, B) = \frac{R}{R+G+B}$, $g(R, G, B) = \frac{G}{R+G+B}$, $b(R, G, B) = \frac{B}{R+G+B}$, hue $H(R, G, B) = \arctan\left(\frac{\sqrt{3}(G-B)}{(R-G)+(R-B)}\right)$ and saturation $S(R, G, B) = 1 - \frac{\min(R, G, B)}{R+G+B}$.

2.2 The Reflection Model

Consider an image of an infinitesimal surface patch. Using the red, green and blue sensors with spectral sensitivities given by $f_R(\lambda)$, $f_G(\lambda)$ and $f_B(\lambda)$ respectively, to obtain an

image of the surface patch illuminated by a SPD of the incident light denoted by $e(\lambda)$, the measured sensor values will be given by Shafer [9]:

$$C = m_b(\vec{n}, \vec{s}) \int_{\lambda} f_C(\lambda) e(\lambda) c_b(\lambda) d\lambda + m_s(\vec{n}, \vec{s}, \vec{v}) \int_{\lambda} f_C(\lambda) e(\lambda) c_s(\lambda) d\lambda \quad (1)$$

for $C = \{R, G, B\}$ giving the C th sensor response. Further, $c_b(\lambda)$ and $c_s(\lambda)$ are the albedo and Fresnel reflectance respectively. λ denotes the wavelength, \vec{n} is the surface patch normal, \vec{s} is the direction of the illumination source, and \vec{v} is the direction of the viewer. Geometric terms m_b and m_s denote the geometric dependencies on the body and surface reflection respectively.

Considering dichromatic reflectance and "white" illumination, then $e(\lambda) = e$ and $c_s(\lambda) = c_s$. The measured sensor values are then:

$$C_w = em_b(\vec{n}, \vec{s})k_C + em_s(\vec{n}, \vec{s}, \vec{v})c_s \int_{\lambda} f_C(\lambda) d\lambda \quad (2)$$

for $C_w \in \{R_w, G_w, B_w\}$ giving the red, green and blue sensor response under the assumption of a white light source. $k_C = \int_{\lambda} f_C(\lambda) c_b(\lambda) d\lambda$ is a compact formulation depending on the sensors and the surface albedo.

If the integrated white condition holds (as we assume throughout the paper):

$$\int_{\lambda} f_R(\lambda) d\lambda = \int_{\lambda} f_G(\lambda) d\lambda = \int_{\lambda} f_B(\lambda) d\lambda = f \quad (3)$$

we have:

$$C_w = em_b(\vec{n}, \vec{s})k_C + em_s(\vec{n}, \vec{s}, \vec{v})c_s f \quad (4)$$

In the next section, this reflection model will be used to study the behavior of the different color spaces in RGB -color space.

2.3 Reflection with White Illumination

2.3.1 Photometric Invariant Color Features for Matte, Dull Surfaces

Consider the body reflection term of eq. (4):

$$C_b = em_b(\vec{n}, \vec{s})k_C \quad (5)$$

for $C_b \in \{R_b, G_b, B_b\}$ giving the red, green and blue sensor response of a matte, dull surface patch under the assumption of a white light source.

According to the body reflection term, the color depends only on k_C (i.e. sensors and surface albedo) and the brightness on factor $em_b(\vec{n}, \vec{s})$. Then the observed colors of a matte, dull surface with fixed k_C can be represented by the color cluster vector \vec{B} , see Figure 1, where the direction of \vec{B} is based on k_C and its extent by $em_b(\vec{n}, \vec{s})$. As a consequence, a uniformly painted surface (i.e. with fixed k_C) may give rise to a broad variance of RGB values due to the varying circumstances induced by the image-forming process such as a change in object orientation, illumination intensity and position. Hence,

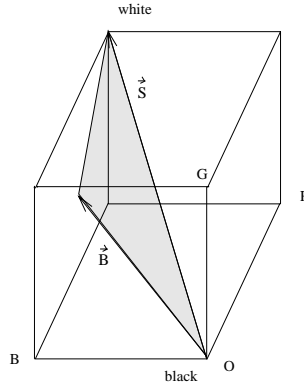


Figure 1: Color cluster vector \vec{B} of a matte surface in RGB , and color cluster vector \vec{S} of a shiny surface in RGB .

all linear combinations of RGB are sensitive to the image-forming process such as I , CMY , XYZ , and $I_1 I_2 I_3$.

In contrast, normalized color rgb is insensitive to surface orientation, illumination direction and intensity as can be seen from:

$$r(R_b, G_b, B_b) = \frac{em_b(\vec{n}, \vec{s})k_R}{em_b(\vec{n}, \vec{s})(k_R + k_G + k_B)} = \frac{k_R}{k_R + k_G + k_B} \quad (6)$$

only dependent on the sensors and the surface albedo. Equal arguments hold for g and b .

Saturation S is an invariant for the set of matte, dull surfaces illuminated by white SPD mathematically specified by:

$$S(R_b, G_b, B_b) = 1 - \frac{\min(em_b(\vec{n}, \vec{s})k_R, em_b(\vec{n}, \vec{s})k_G, em_b(\vec{n}, \vec{s})k_B)}{em_b(\vec{n}, \vec{s})(k_R + k_G + k_B)} = 1 - \frac{\min(k_R, k_G, k_B)}{(k_R + k_G + k_B)} \quad (7)$$

Similarly, hue H is an invariant for matte, dull surfaces:

$$H(R_b, G_b, B_b) = \arctan\left(\frac{\sqrt{3}em_b(\vec{n}, \vec{s})(k_G - k_B)}{em_b(\vec{n}, \vec{s})((k_R - k_G) + (k_R - k_B))}\right) = \arctan\left(\frac{\sqrt{3}(k_G - k_B)}{(k_R - k_G) + (k_R - k_B)}\right) \quad (8)$$

In fact, any expression defining colors on the same linear color cluster spanned by the body reflection vector in RGB -space is an invariant for the dichromatic reflection model with white illumination. To that end, we put forward the following invariant color model:

$$c_1 = \arctan\left(\frac{R}{\max\{G, B\}}\right), c_2 = \arctan\left(\frac{G}{\max\{R, B\}}\right), c_3 = \arctan\left(\frac{B}{\max\{R, G\}}\right) \quad (9)$$

denoting the angles of the body reflection vector and consequently being invariants for matte, dull objects:

$$c_1(R_b, G_b, B_b) = \arctan\left(\frac{em_b(\vec{n}, \vec{s})k_R}{\max\{em_b(\vec{n}, \vec{s})k_G, em_b(\vec{n}, \vec{s})k_B\}}\right) = \arctan\left(\frac{k_R}{\max\{k_G, k_B\}}\right) \quad (10)$$

only dependent on the sensors and the surface albedo. Equal arguments hold for c_2 and c_3 .

Obviously, in practice, the assumption of objects composed of matte, dull surfaces is not always realistic. To that end, the effect of surface reflection (highlights) is discussed in the following section.

2.3.2 Photometric Invariant Color Features for Both Matte and Shiny Surfaces

Consider the surface reflection term of eq. (4):

$$C_s = em_s(\vec{n}, \vec{s}, \vec{v})f \quad (11)$$

for $C_s \in \{R_s, G_s, B_s\}$ giving the red, green and blue sensor response for a highlighted surface patch with white illumination.

Note that under the given conditions, the color of highlights is not related to the color of the surface on which they appear, but only on the color of the light source. Thus for the white light source, the surface reflection color cluster \vec{S} is on the diagonal grey axis of the basic RGB -color space corresponding to intensity I , see Figure 1.

For a given point on a shiny surface, the contribution of the body reflection component C_b and surface reflection component C_s are added together $C_w = C_s + C_b$. Hence, the observed colors of the surface must be inside the triangular color cluster in the RGB -space formed by the two reflection components, see Figure 1.

Because H is a function of the angle between the main diagonal and the color point in RGB -sensor space, all possible colors of the same (shiny) surface region (i.e. with fixed albedo) have to be of the same hue as follows from substituting eq. (4) in the hue equation:

$$H(R_w, G_w, B_w) = \arctan\left(\frac{\sqrt{3}(G_w - B_w)}{(R_w - G_w) + (R_w - B_w)}\right) = \arctan\left(\frac{\sqrt{3}em_b(\vec{n}, \vec{s})(k_G - k_B)}{em_b(\vec{n}, \vec{s})((k_R - k_G) + (k_R - k_B))}\right) = \arctan\left(\frac{\sqrt{3}(k_G - k_B)}{(k_R - k_G) + (k_R - k_B)}\right) \quad (12)$$

factoring out dependencies on illum. e , object geometry $m_b(\vec{n}, \vec{s})$, viewpoint $m_s(\vec{n}, \vec{s}, \vec{v})$, and specular reflection coefficient c_s and hence only dependent on the sensors and the surface albedo. Note that $R_w = em_b(\vec{n}, \vec{s})k_R + em_s(\vec{n}, \vec{s}, \vec{v})c_s f$, $G_w = em_b(\vec{n}, \vec{s})k_G + em_s(\vec{n}, \vec{s}, \vec{v})c_s f$, and $B_w = em_b(\vec{n}, \vec{s})k_B + em_s(\vec{n}, \vec{s}, \vec{v})c_s f$.

In fact, any expression defining colors on the same linear triangular color cluster, formed by the two reflection components in RGB -space, are photometric color invariants for the dichromatic reflection model.

To that end, a new photometric color invariant model is proposed uniquely determining the direction of the linear triangular color cluster:

$$l_1(R, G, B) = \frac{(R - G)^2}{(R - G)^2 + (R - B)^2 + (G - B)^2}, l_2(R, G, B) = \frac{(R - B)^2}{(R - G)^2 + (R - B)^2 + (G - B)^2}, l_3(R, G, B) = \frac{(G - B)^2}{(R - G)^2 + (R - B)^2 + (G - B)^2} \quad (13)$$

the set of normalized color differences which is, similar to H , an invariant for the set of matte and shiny surfaces as follows from substituting eq. (4) in l_1 , l_2 and l_3 .

3 Segmentation Methods

Two segmentation methods are taken to examine the effect of the different color models for the purpose of robust color image segmentation: a clustering and a region growing technique. The clustering technique clusters pixels on basis of the different color model features present in an image according to the k-means algorithm [4]. The other approach is derived from the split& merge algorithm proposed by Horowitz and Pavlidis [6].

3.1 Clustering Technique

The k-means method is based on the minimization of the so-called *performance index* defined as the sum of squared distances of all pixels to their cluster means. First an initial partition is given, obtained by assigning each pixel to its closest cluster mean, on basis of the Euclidean distance measure, and new partitions are obtained by moving pixels from one cluster to another until the performance index is reduced to its minimum. The determination of initial cluster means plays a crucial part, because the initial partition is obtained by assigning pixels to their closest cluster means and the better the initial partition is, the faster the k-means method will converge.

A more detailed version is as follows:

STEP 1: $s = 1$; determine k initial cluster means $\vec{c}_1(s), \vec{c}_2(s), \dots, \vec{c}_k(s)$, corresponding to k important patterns in the data;

STEP 2: During the s^{th} iteration each pixel \vec{a} is assigned to one of the k clusters $C_1(s), C_2(s), \dots, C_k(s)$: \vec{a} is assigned to cluster $C_j(s)$ if $\|\vec{a} - \vec{c}_j(s)\| < \|\vec{a} - \vec{c}_i(s)\|$, $\forall i, j = 1, 2, \dots, k \wedge i \neq j$;

STEP 3: Recomputation of k new cluster means: $\vec{c}_j(s+1) = \frac{1}{N_j} \sum_{\vec{a} \in C_j(s)} \vec{a}$, $j = 1, 2, \dots, k$;

STEP 4: if $\exists j \in \{1, \dots, k\} \vec{c}_j(s+1) \neq \vec{c}_j(s)$ then $s = s + 1$; **GOTO STEP 2**; else **STOP**.

where $\vec{c}_j(s)$ indicates the cluster mean of the j^{th} cluster after s iterations, $C_j(s)$ denotes the j^{th} cluster after s iterations with cluster mean $\vec{c}_j(s)$, \vec{a} is a pixel described by a n -dimensional feature vector and N_j is the number of pixels of cluster $C_j(s)$.

In order to determine the initial cluster means, a n -dimensional histogram is generated and k cluster means, corresponding to k conspicuous peaks in the histogram, are computed. The number of clusters must be known in advance.

3.1.1 Clustering by Fitting Lines (Matte Objects) or Planes (Shiny Objects) Through *RGB*-data

For the k-means clustering method, similarity defined on a cluster C_j will be true if pixels in that cluster have similar values. This definition hold for color invariant models. However, an alternative way is to cluster on straight lines originating from the origin in *RGB*-color space. This can be seen as follows. According to the body reflection model given by eq. (5), the observed colors of a matte, dull surface with fixed k_C are represented by the color cluster vector \vec{B} , see Figure 1. Therefore, we propose that the alternative similarity measure is defined by fitting lines originating at $(0, 0)$ to the observed colors in the *RGB*-color cube. To illustrate this, we consider the image in Figure 2. The image is

taken from printed textile with 4 different colors. As one can see, four linear clusters are produced in RGB -color space originating from the origin (black). Note that the k-means clustering method has nicely fit four straight lines originating at $(0, 0)$ to the RGB -data, yielding four clusters independent of the imaging conditions.

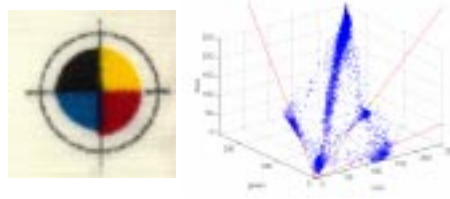


Figure 2: a. Color image taken from printed textile. b. Observed colors in the RGB -color cube.

Similarly, to find homogeneous colored *shiny* surfaces, we propose an alternative similarity measure which is based on fitting planes, originating at the diagonal axis, to the observed colors in the RGB -color cube. In other words, a region is considered to be homogeneous if the RGB -colors form a planar plane, see Figure 1, which falls within the limit of the mean image noise standard deviation, in the RGB -color cube originated at diagonal axis.

3.2 Split and Merge Technique

First, color feature images are computed from the original R , G and B values of the red, green, and blue images. During the second step the image, where each pixel is a n - dimensional color feature vector, will be partitioned into square regions of equal size, corresponding to the conversion of the image into the initialization level of the quadtree. The third step will merge four quadrants together into one quadrant when the resulting quadrant satisfies a certain homogeneity condition and one quadrant will be split into four quadrants if the quadrant does not satisfy a homogeneity condition. The fourth step in the processing sequence is necessary in order to group adjacent quadrants, because intrinsic homogeneous objects or object surfaces might not exactly fit within a quadrant. During the 5th step small regions will be eliminated because there may be still a large number of small regions to be left. The final segmentation result will be computed in the 6th step, yielding a contour image where each contour corresponds to objects or object surface boundaries.

The homogeneity criterion is based on the variance and the mean of a particular region R . Hence, the hypothesis is that the pixels of region R have constant intensity values. a_{ij} indicating the value of pixel i of the j^{th} color feature and ma_j denoting the mean of the j^{th} color feature: $ma_j = \frac{1}{m} \sum_{i=1}^m a_{ij}$, where m is the number of pixels in the particular region. The variance is defined is given by $V_j = \frac{1}{m} \sum_{m=i}^m (a_{ij} - ma_j)^2$. The mean and variance homogeneity criterion defined over a connected set of pixels (region)

$$R \text{ is: } P(R) = \begin{cases} \mathbf{F}, & \text{if } \sqrt{(V_1)^2 + (V_2)^2 + \dots + (V_n)^2} > e \\ \mathbf{T}, & \text{OTHERWISE} \end{cases}, \text{ where } e$$

is a given threshold.

4 Experiments

In this section, we evaluate and compare the performance of the various color features for the purpose of color invariant image segmentation.

Figure 3.a is a color image of several toys against a background consisting of four squares. Objects were recorded in 3 RGB -colors with the aid of the SONY XC-003P CCD color camera (3 chips) and the Matrox Magic Color frame grabber. The digitization was done in 8 bits per color. Two light sources of average day-light color were used to illuminate the objects in the scene. The size of the image is 256×256 . The first upper left quadrant consists of three uniformly painted matte cubes of wood. The second upper right quadrant contains two specular plastic donuts on top of each other. In the bottom left quadrant a red highlighted ball and a matte cube are shown while the last quadrant contains two matte cubes. Note that each individual object is painted uniformly with a distinct color. The image is contaminated by a substantial amount of noise, shadows, shading, inter-reflections and specularities. Inter-reflections occur when an object receives the reflected light from other objects.



Figure 3: Segmentation results for the split and merge method differentiated for the various color models RGB , S , rgb and $l_1l_2l_3$ computed from the recorded color image shown in Figure 3.a. a. Color image. b. RGB -segmentation result. c. S -segmentation result. d. rgb -segmentation result. e. $l_1l_2l_3$ -segmentation result. Note that only $l_1l_2l_3$ produce region edges corresponding to material transitions.

In Figure 3 segmentation results are shown obtained by the split and merge technique. In Figure 3.b segmentation result is shown obtained from RGB -values. Clearly, false regions are introduced by abrupt surface orientations, shadows, inter-reflections and highlights. In contrast, computed regions for S and rgb shown in Figure 3.c and 3.d respectively are insensitive for shadows, illumination and surface orientation changes but affected by inter-reflections (e.g. caused by the donuts and the background) and highlights (S more than r). S is more sensitive to noise. rgb and S provide poor segmentation results in areas where intensity is small (i.e. within 5% of the total intensity range). Good performance is shown for $l_1l_2l_3$ shown in 3.e, where computed region edges correspond to material boundaries discounting the disturbing influences of surface orientation, illumination, shadows and highlights. Inter-reflections disturb the quality of the segmentation result slightly. Poor segmentation results are provided by $l_1l_2l_3$ in areas where the intensity and saturation is small ($\leq 5\%$ of the total range).

We now consider the segmentation results obtained by the kmeans algorithm differ-

entiated for the various color models. In order to determine the initial cluster means, a 3-dimensional histogram is generated and k cluster means, corresponding to k conspicuous peaks in the histogram, are computed. The number of clusters for the color image at hand is $k = 7$.

In Figure 4.b and 4.c segmentation results are shown obtained by the kmeans clustering method on I and RGB respectively. Clearly, false regions are introduced by abrupt surface orientations, shadows, inter-reflections and highlights. Similar observations can be made for the Figures 4.c-h showing the results based on XYZ , YIQ , $I_1I_2I_3$, IHS , and Lab . It can be seen that all color models including intensity (brightness) in their systems are sensitive to surface orientations, shadows, and highlights. In contrast, computed regions for rgb , xyz and $c_1c_2c_3$ (normalized to intensity) shown in Figure 4.i, 4.j and 4.k respectively are insensitive for shadows and surface orientation changes but are affected by highlights. Similar results are obtained by fitting straight lines through RGB -data, shown in Figure 4.l, by the method described in Section 3.1.1. Poor segmentation results are obtained in areas of the image where intensity is small.

Good performance is shown for $l_1l_2l_3$ and H shown in 4.m and 4.n respectively, where computed region edges neatly correspond to material boundaries discounting the disturbing influences of surface orientation, illumination, shadows and highlights. Only inter-reflections and low intensity disturb the quality of the segmentation slightly. Similar results are obtained by fitting planes through RGB -data, shown in Figure 4.o, by the method described in Section 3.1.1.

5 Conclusion

The goal of this paper is to detect regions discounting the disturbing influences of surface orientation change, illumination, shadows and highlights.

On the basis of the theoretical and experimental results it is concluded that color models $l_1l_2l_3$, H , S , $c_1c_2c_3$, rgb and xyz are all invariant to a change in surface orientation, viewpoint of the camera, and illumination intensity. Same invariant properties hold for fitting straight lines to colors in the RGB -color cube. In addition, $l_1l_2l_3$ and H are also insensitive to highlights. Same highlight invariant property holds for fitting planes to colors in the RGB -color cube.

A major drawback of the above systems is that they provide poor segmentation results when intensity (S , rgb and xyz) and saturation ($l_1l_2l_3$ and H) is small. Linear combinations of the RGB such as I , CMY , YIQ , XYZ , and $I_1I_2I_3$ all heavily depend on surface orientation and illumination intensity in addition to color models incorporating brightness into their systems: I in HSI , L^* in $L^*a^*b^*$, and L in Luv .

References

- [1] Bajcsy, R., Lee S. W., and Leonardis, A., *Color Image Segmentation with Detection of Highlights and Local Illumination Induced by Inter-reflections*, In IEEE 10th ICPR'90, pp. 785-790, Atlantic City, NJ, 1990.
- [2] Celenk, M., *A Color Clustering Technique for Image Segmentation*, CVGIP, No. 52, pp. 145-170, 1990.
- [3] Gevers, T. and Smeulders, A. W. M., *Image Indexing using Composite Color and Shape Invariant Features*, ICCV, Bombay, India (1998)

- [4] Hartigan, J. A., *Clustering Algorithms*, John Wiley and Sons, U.S.A., 1975.
- [5] Healey, G., *Segmenting Images Using Normalized Color*, IEEE Syst., Man. Cybern., Vol. 22, pp. 64-73, 1992.
- [6] Horowitz, S. L. and Pavlidis, T., *Picture Segmentation by a Directed Split-and-Merge Procedure*, In Proc. 2nd Int. Joint Conf. on Pattern Recog., Copenhagen, pp. 424-433, 1974.
- [7] Klinker, G. J., Shafer, A. and Kanada, T. *A Physical Approach to Color Image Understanding*, Int. J. of Comp. Vision, Vol. 4, pp. 7-38, 1990.
- [8] Liu, J. and Yang, Y-H., *Multi-resolution Color Image Segmentation*, IEEE PAMI, Vol. 16, No. 7, pp. 689-700, 1994.
- [9] Shafer, S. A., *Using Color to Separate Reflection Components*, COLOR Res. Appl., 10(4), pp 210-218, 1985.

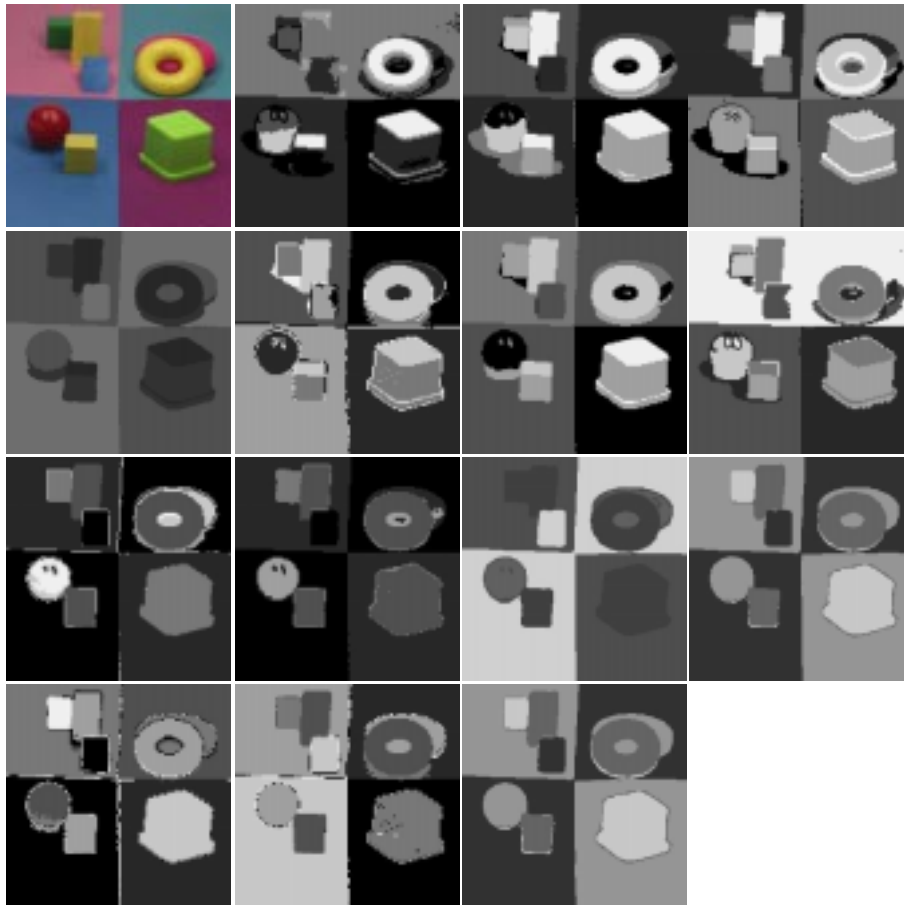


Figure 4: Segmentation results for the *kmeans* clustering method. *a.* Color image. *b.* *I*-segmentation result. *c.* RGB. *d.* XYZ *e.* YIQ. *f.* $I_1I_2I_3$. *g.* IHS. *h.* Lab. *i.* rgb. *j.* xyz. *k.* $c_1c_2c_3$. *l.* Fitting lines through RGB-data. *m.* $l_1l_2l_3$. *n.* H. *o.* Fitting planes through RGB-data.